AD_____

Award Number: W81XWH-08-1-0613

TITLE: X-Ray Phase Imaging For Breast Cancer Detection

PRINCIPAL INVESTIGATOR: Xizeng Wu, Ph.D.

CONTRACTING ORGANIZATION: University of Alabama at Birmingham
Birmingham, AL 35294

REPORT DATE: September 2011

TYPE OF REPORT: Annual

PREPARED FOR: U.S. Army Medical Research and Materiel Command
Fort Detrick, Maryland 21702-5012

DISTRIBUTION STATEMENT: Approved for Public Release;
Distribution Unlimited

REPORT DOCUMENTATION PAGE

Form Approved
OMB No. 0704-0188

1. REPORT DATE	2. REPORT TYPE	3. DATES COVERED
September 2011	Annual	1 September 2010 – 31 August 2011

4. TITLE AND SUBTITLE

X-Ray Phase Imaging For Breast Cancer Detection

5a. CONTRACT NUMBER

5b. GRANT NUMBER
W81XWH-08-1-0613

5c. PROGRAM ELEMENT NUMBER

6. AUTHOR(S)

Xizeng Wu, Ph.D.

E-Mail: xwu@uabmc.edu

5d. PROJECT NUMBER

5e. TASK NUMBER

5f. WORK UNIT NUMBER

7. PERFORMING ORGANIZATION NAME(S) AND ADDRESS(ES)

University of Alabama at Birmingham
Birmingham, AL 35294

8. PERFORMING ORGANIZATION REPORT NUMBER

9. SPONSORING / MONITORING AGENCY NAME(S) AND ADDRESS(ES)
U.S. Army Medical Research and Materiel Command
Fort Detrick, Maryland 21702-5012

10. SPONSOR/MONITOR'S ACRONYM(S)

11. SPONSOR/MONITOR'S REPORT NUMBER(S)

12. DISTRIBUTION / AVAILABILITY STATEMENT
Approved for Public Release; Distribution Unlimited

13. SUPPLEMENTARY NOTES

14. ABSTRACT
The long term objective of the project is to develop a low-dose and quantitative phase x-ray imaging technique for facilitating breast cancer detection. In this period we have accomplished following tasks: 1) We compared the robustness of the phase retrievals with two phase-retrieval methods, as the common TIE-based method vs. the AP-based method that we developed, by analyzing the phase maps retrieved from the experimental images of a phantom. The AP-based method is shown in the experiment to be superior to the TIE-based method for the robustness in performing the phase retrieval. (2) We conducted phantom imaging studies with 100 kVp-140 kVp tube voltages and performed the phase retrievals to retrieve phantom phase maps for fully exhibiting the phase contrast and providing quantitative information on the phantom electron densities. The results of the study show that the phase contrast exhibited in the retrieved phase maps compensates for the attenuation-contrast loss associated with the high tube-voltages, and with these techniques the radiation doses are reduced and quantitative information on the phantom projective electron densities is obtained. In the coming no-cost extension period, We plan to further optimize the design trade-off in image detection for achieving more large radiation dose reductions and refine our phase retrieval method for higher retrieval accuracies.

15. SUBJECT TERMS
Phase-contrast x-ray imaging, Breast imaging, Phase retrieval

16. SECURITY CLASSIFICATION OF:			17. LIMITATION OF ABSTRACT	18. NUMBER OF PAGES	19a. NAME OF RESPONSIBLE PERSON
a. REPORT	b. ABSTRACT	c. THIS PAGE			USAMRMC
U	U	U	UU	24	19b. TELEPHONE NUMBER *(include area code)*

Table of Contents

Introduction

Conventional mammography is limited in its sensitivity for detecting subtle breast pathological changes, since the imaging relies on the small differences in x-ray attenuation between the lesions and breast tissues. As x-ray traverses a breast, it gets not only attenuated, but also phase-shifted. Utilizing the highly sensitive x-ray phase-shifts, the phase sensitive x-ray imaging has the potential of greatly increasing x-ray imaging sensitivity and specificity and reducing radiation doses associated with the imaging.

The long term objective of the project is to develop a low-dose and quantitative x-ray phase imaging technique for facilitating breast cancer detection. The Specific Aims of the project of the three-year period are: (1) Develop a prototype phase-imaging system enabling the phase retrieval, that is, the reconstruction of objects phase-maps. The system hardware comprises a micro-focus tube operating at high tube voltages, a high resolution photostimulable phosphor plate (CR-plate) based detector system. The core algorithms for breast phase-map reconstruction will be developed to retrieve a breast phase map from a single recorded image. (2) Validate the accuracy of the reconstructed tissue projected electron densities; validate the many-fold radiation dose reduction achieved with the proposed system; conduct subjective measurements to characterize the performance of the proposed system.

Body

In this period we have performed following studies: (A) Since the robustness of phase retrieval methods is of critical importance for limiting and reducing radiation doses involved in x-ray phase imaging, in this period we have compared the robustness of the attenuation-partition based (AP-based) phase retrieval method that we developed to robustness of the Transport of Intensity Equation based (TIE-based) method. (B) In order to develop low-dose and quantitative x-ray phase imaging, in this period we have conducted phantom imaging studies with 100 kVp-140 kVp tube voltages and performed the phase retrievals to retrieve phantom phase maps for fully exhibiting the phase contrast and providing quantitative information on the phantom electron densities.

(A). Experimental performance evaluation of the attenuation-partition based iterative phase retrieval method

Introduction: In the Period 2 we developed a novel phase retrieval method, the attenuation-partition based (AP-based) iterative phase retrieval method. The phase retrieval is a procedure of retrieving the phase-shift map $\varphi(\vec{r})$ of an object from its phase-sensitive projections, where $\varphi(\vec{r}) = -\lambda r_e \int_{ray} \rho_e(\vec{r}, s)ds$ and $\rho_e(\vec{r}, s)$ denotes the tissue electron density, $r_e =$ 2.818 x 10^{-15} m is the classical electron radius and λ is x-ray wavelength, the integral is computed over the ray path. A retrieved phase map is able to fully exhibit tissue phase contrast and provide a quantitative map of the object's projected electron densities, which could be used for quantitative tissue characterizations. Moreover, performing phase retrieval is necessary for reconstructing volumetric 3-D maps of tissue attenuation coefficients and refractive indices

respectively, and for eliminating the phase-contrast caused artifacts in the volumetric 3-D images.

Examining the robustness of phase retrieval methods against the projection noise, such as the x-ray photon quantum noise involved in the projection acquisitions, is an important task in developing phase imaging techniques for future medical imaging applications. If a phase retrieval method is not robust against the noise, the method could become unstable and fail for phase retrieval if the acquired projection images were contaminated with substantial noise. On the other hand, suppressing x-ray quantum noise may require using high radiation doses in the image acquisitions. For clinical applications it is imperative to limit and reduce radiation doses involved, hence it is critical to develop robust phase retrieval methods for future clinical applications of phase contrast imaging. The most commonly used method for phase retrieval in the literature is based on the Transport of Intensity Equation (TIE) for phase contrast projections [Allen et al. 2001]. While the TIE-based phase retrieval method is computational effective for the cases with strong phase contrast effects and low noise levels, we found that it would fail for phase retrieval when the acquired projection images were contaminated with relatively strong noises as in clinical applications where radiation dose constraints dictates relatively high noise levels. To improve the robustness of phase retrieval, we recently developed a novel method called the attenuation partition (AP) based method, or the AP-based method for short. In this period we compared the robustness of two phase-retrieval methods, as the TIE-based method vs. the AP-based method, by analyzing the phase maps retrieved from the experimental images of a phantom.

Method: We applied these two methods to experimental projection images of an air-bubble wrap phantom for retrieving the phase map of the bubble wrap. According to the TIE-based method, one acquires two images: one contact radiograph, and one phase contrast image. The phase map $\varphi(\vec{r})$ is retrieved as $\varphi(\vec{r}) = -(2\pi M/\lambda R_2)\nabla^{-2}\left\{\nabla\cdot\left[\nabla\left(\nabla^{-2}\left(M^2 I/I_{in} - A_o^2\right)\right)\Big/A_o^2\right]\right\}$ [Allen et al. 2001], where A_o^2 denotes the its x-ray attenuation map of an object obtained from its contact radiograph, λ is the average x-ray wavelength, I the phase-sensitive projection intensity, I_{in} the entrance x-ray intensity, R_1 the source-object distance set in the projection, R_2 is the object-detector distance and $M = (R_1 + R_2)/R_1$ the magnification factor in the projection. In above formula the operator ∇ denotes the two-dimensional transverse gradient differential operator, and ∇^{-2} denotes the inverse Laplacian operator. We noted that the Achilles heel of the TIE-based method lies at the inverse Laplacian operator ∇^{-2} involved in the method. This singularity may amplify the noise randomly embedded in the acquired images and result in instability in phase retrievals. To mend the instability of the TIE-method, one may use the Tikhonov regularization technique, which regularizes the inverse Laplacian operator ∇^{-2} attempting to tame the singularity-caused problems, but its effectiveness is very limited [Allen et al. 2001],

In order to get rid of the singular pseudo-differential operator ∇^{-2} involved in the TIE-based phase retrievals, we recently developed a novel phase retrieval method: the AP method. Our idea is to utilize the correlation between the x-ray phase shift and its attenuation to eliminate the singularities involved in phase retrievals. According to this the AP-based method, one first applies the duality transform $\mathfrak{D}$ to the acquired phase contrast image $I(\vec{r})$ to obtain an estimate of both the Compton scattering-generated attenuation A_{KN}^2 and phase map $\varphi(\vec{r})$ of the sample. Here the duality transform $\mathfrak{D}$ is implemented by using the pseudo-differential operator

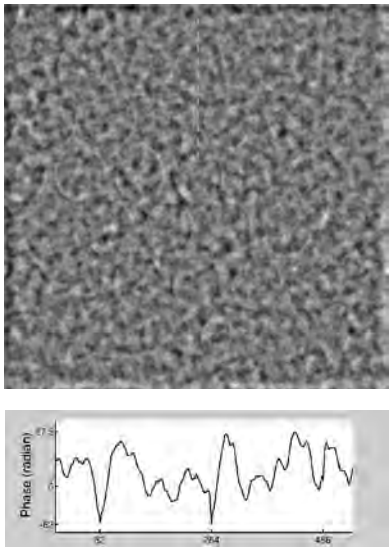

Fig. 1. (Upper) Retrieved phase maps of the bubble wrap with the TIE-based method and mended with the Tikhonov regularization. (Lower) Profile of the retrieved phase values along the marked line.

$\mathfrak{D}(I) \equiv \left(1 - \left(\lambda^2 R_2 r_e / 2\pi M \sigma_{KN}\right)\nabla^2\right)^{-1} \cdot \left(M^2 I / I_{in}\right)$, where σ_{KN} denotes the average Compton scattering cross-section, r_e the classical electron radius the phase-attenuation duality [Wu et al. 2005,]. One then compares A_{KN}^2 against the acquired normalized radiograph A_o^2 and computes their differences as the error δA. Applying the Fresnel diffraction transform $\mathfrak{F}_{\tau\varepsilon}$ to the fictitious transmission function $\delta A \cdot \exp(i\varphi)$, one computes a better estimates of I_{KN}, the projection intensity determined by using the estimated object's electron densities and counting only the Compton scattering-generated attenuation. With this new estimate of I_{KN} one can start a new round of the iteration to compute a new improved estimates of both the A_{KN}^2 and phase map $\varphi(\vec{r})$ of the sample. The iteration converges when the I_{KN} does not change substantially with further iteration steps.

In order to compare the robustness of the AP-based method against the TIE-based method, we applied the two methods for retrieving the phase-map of a piece of air bubble wrap. The x-ray tube employed was with a 7-μm focal spot. A contact radiograph and a phase contrast image were all acquired with 40 kVp, 6 mAs and a source-detector distance of 1.78 m. However, the phase contrast image was acquired with a large sample-detector distance of 1.15 m for allowing the exiting x-rays to freely diffract over a long distance and form the interference fringes. The imaging detector employed was an aSe-based flat-panel detector with a pixel pitch of 140 μm. Using the acquired radiograph and phase contrast image, the phase maps of the bubble wrap were retrieved with the two methods, as shown in Fig. 1 (with the TIE based method) and Fig. 2 (with the AP-based method.), respectively. The image qualities and the phase-values profiles of the two retrieved phase maps were analyzed for examining the robustness of the two methods.

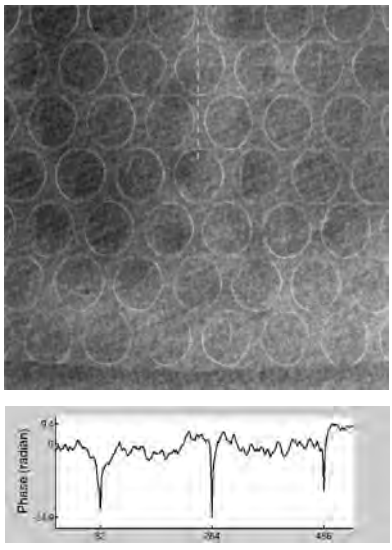

Fig. 2. (Upper) Retrieved phase maps of the bubble wrap with the AP-based method. (Lower) Profile of the retrieved phase values along the marked line.

Result: Fig. 1-(upper) shows the retrieved sample's phase map using TIE-based method . Apparently the retrieval with the TIE-based method is very unsatisfactory, as the bubble rims are hardly visible in the extremely cluttered background in the phase map. In a stark contrast to the TIE-based method, the bubble rims are prominently depicted in Fig. 2-(upper), which was retrieved using the AP-method. In order to gauge the accuracies of the retrieved phase values, we measured the thicknesses of the flat bases of the wrap using a caliber ruler, and we found that the base thickness was about 0.055 mm. The wrap base is made of the low-density polyethylene films. According to the film's molecular formula $(C_2H_4)_n$ and its mass density is 0.925 g/cm^3, we found that the approximate phase-shifts at the flat bases of the wrap is about -4.2 radian. On the other hand, according to the phase profile in Fig. 2(lower) with

the AP-based method, the average phase shift at the flat bases of the wrap is -1.05 radian, the two phase-shift estimates are reasonably close. In comparison, the phase profile in Fig. 1(lower) with the TIE-based method, depicts just messy up-down peaks buried in cluttered and noisy background. According to this profile, the phase-shift values at the bases fluctuate over a wide range from 0 to +87.5 radian with an average of +27.3 radian, contradicting to the fact that x-ray phase shifts should be negative.

In summary, we showed that the TIE-based method failed in retrieving the air bubble wrap's phase map. In contrast, the AP-based method retrieved the wrap phase map successfully. The retrieved phase values with the AP-based are reasonably close to the estimate based on the wrap thickness measurement. The stark performance differences of the two methods are rooted in their different techniques employed to deal with the singularity problem in phase retrievals. This comparison shows that the conventional TIE-based phase retrieval method is unstable against the noise in the wrap's projection images, while the AP-based phase retrieval method is shown in the experiment to be superior to the TIE-based method for the robustness in performing the phase retrieval.

In addition, extending the research work on the phase retrieval methods, as a by-product of this project, we made a progress in understanding the apparent linear attenuation coefficients in the inline phase contrast tomography. In the inline phase contrast x-ray tomography the reconstructed apparent linear attenuation coefficient values in the tomography may be greatly larger than sample's linear attenuation coefficients or even be negative. These "artifacts" may cause faulty interpretation of sample structures, and impede even qualitative characterizations for tissues and materials. In this period we derived a general formula to quantitatively relate the apparent linear attenuation coefficient values in cone-beam phase contrast tomography to sample's linear attenuation coefficients and refractive indices [Yan and Wu 2011]. This formula overcomes the gross inaccuracy of the existing formula in the literature in analyzing high-resolution phase contrast tomography, and it will be useful for correctly interpreting and quantifying the apparent linear attenuation coefficients in cone-beam x-ray phase contrast tomography in the biomedical and material science applications.

(B). Develop low-dose and quantitative x-ray phase imaging techniques

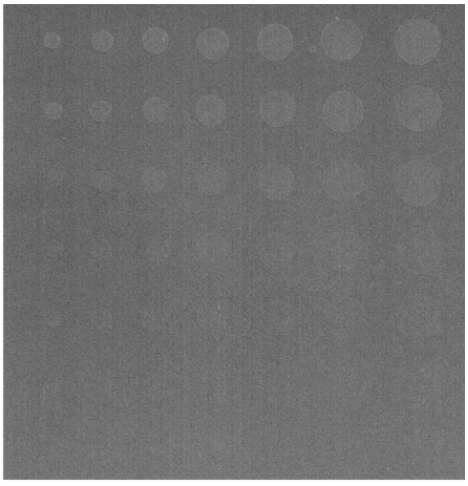

Fig. 3. Phase contrast image of a contrast-detail phantom acquired with 120 kVp and M =2.

Introduction: As conventional mammography (digital or screen/film) employs low tube voltages (25-32 kVp) for breast imaging, we conducted phantom imaging studies with 100 kVp-140 kVp tube voltages in this period for developing low-dose and quantitative x-ray phase imaging techniques. Our strategy is to utilize the phase contrast to compensate for the attenuation-contrast loss associated with the high tube-voltages, and to accomplish the radiation doses reduction with the high-voltage phase imaging.

Method: The prototype system hardware consists of a micro-focus x-ray tube (Hamamatsu L8121-03) with a focal spot of 50 μm for 75 W power loading, and operating at voltages up to 150 kVp, and a high-resolution (43.75 um) CR system (Konica Minolta). We have conducted preliminary imaging experiments using 100, 120, 140 kVp and with four different phantoms, the ACR MAP phantom,

a contrast-detail phantom, an acrylic step-edge, and a breast tissue-equivalent phantom. We images the phantoms with different geometric configurations including the settings with magnification factors of 1, 2, 2.5, 3. Observer studies were performed utilizing the ACR MAP and contrast-detail phantoms for quantitative comparisons. In this way we seek to validate the optimal geometric configurations for phase contrast visibility as determined in the first period based on the theoretical phase contrast visibility analysis [Wu et al., 2004].

In order to accurately estimate the average glandular doses involved in the experiments, we extended our previous tables of the normalized average glandular doses (D_{gN}) for the conventional mammography to the D_{gN} values for the high energy x-rays, by performing the Monte Carlo simulations of x-ray photon transport and energy deposition in breast tissues.

In order to fully exhibit tissue phase contrast and provide a quantitative information of the imaged objects, performing phase retrieval is necessary. While the AP-based phase retrieval method discussed in section (A) is a general method, it needs at least two projection images for phase retrievals. In order to further reduce radiation doses involved, a phase retrieval method requires only one single phase-sensitive projection would be even more desirable. Considering the facts that breast consists of dominantly soft tissues and the x-rays from tubes operating at 120-150 kVp are dominantly high-energy x-rays (60 keV or higher), we employed a novel method to retrieve the phase map of an object by using just one single phase contrast projection image [Wu et al. 2005, Wu et al. 2009]. According to this method, the phase map of the object can be accurately retrieved by using the duality transform as $\varphi(\vec{r}) = (\lambda r_e / \sigma_{KN}) \ln \mathfrak{D}(I(\vec{r}_D))$, where $\mathfrak{D}(I(\vec{r}_D))$ is the duality transform, as is defined earlier in Section (A), of a phase contrast projection $I(\vec{r}_D)$ of the object

Results: Shown in Fig. 3 is a phase contrast image of a contrast-detail phantom acquired with 120 kVp and a magnification factor of 2. In Fig. 3 the phase contrast is exhibited as the highlighted edges of the test disks. Although phase contrast generally decreases with increasing tube voltages, but this image demonstrates that the phase contrast improves image qualities even for such a high tube-voltage of 120 kVp. The observer study on acquired phase contrast projections with a range of magnification factors from M =2 to M =3 have validated the designs made in the first period for the optimal geometric configurations, which balances the conflict requirements for the x-ray spatial coherence and generating large diffraction fringes in images [Wu et al., 2004]. Fig. 4 shows two images of a ACR MAP phantom acquired with the prototype system. The Fig. 4-(left) is a phase-sensitive projection acquired at 100 kVp and a magnification factor of 2. For comparison, the Fig. 4-(right) shows the contact radiograph of the phantom acquired with the same kVp and the same phantom dose. Both images were acquired without any anti-scatter grid. The loss of the attenuation contrast associated with the high tube voltage is responsible for the poor contrast shown in Fig. 4-(right), though the x-ray scatter contributed to the image contrast degradation as well. In contrast, the phase-sensitive projection image in Fig. 4-(left) scores much better in the visibilities of fibers, specks and masses in the phantom.

In order to fully exhibit the phase contrast of phantom components and provide their projective electron densities, we conducted a phase retrieval study to retrieve phantom phase maps by using our novel phase retrieval method. As an example, shown in Fig. 5 is a phase map of an ACR phantom retrieved by using our duality-based method from a single phase-sensitive projection acquired with the prototype system. The tube voltage used was 120 kVp with an estimated average glandular dose of 98.9 mrad. As is shown in Fig. 5 the phantom phase map scores 4 fibers, 3 specks group, and 3.5 masses for the feature-visibilities.

While this glandular dose is quite low compared to the phantom dose levels of 150-250 mrad commonly used in conventional mammography, we expect much more dose saving can be achieved in future experiments with an improved control of the tube-voltage ramping effects and with a quantum-efficient high resolution detector better matched with the high tube-voltages employed in the project. Currently we are working on these planned improvements. Moreover, Fig. 5 provides as well a map of x-ray phase shifts for different phantom features. For example, from Fig. 5 we found that the phase shift for the acrylic frame of the phantom is -1141 radians, the phase shift from the base of wax-insert (including the acrylic substrate) is -1096 radians, and the phase shift from acrylic body and the first mass is -1106 radians. Note that x-ray phase shifts are given by the formula $\varphi = -\lambda r_e \int_{ray} \rho_e(s)ds$ as is explained in Section (A), hence x-ray phase shifts should be of negative values. Hence increasing electron densities or increasing ray path lengths in tissues will generate more negative phase shift values. The three retrieved phase values mentioned above are obviously consistent with the notion of the phase-shifts. We have checked the accuracies of these retrieved phase values against the phase-shift estimates for 60 keV x-rays using the ray tracing modeling for a digital model of the ACR MAP phantom that we built, under the assumption that the x-rays in the experiment have an average energy of 60 keV. The ray-tracing based estimates give the phase values of -923 radians, -879 radians, -887 radians for the acrylic frame, wax-insert base and the first mass, respectively. The retrieved phase values differ by 23% to 25% from these ray-tracing based estimates. This preliminary comparison shows that the accuracies of these retrieved phase values are reasonable good, especially considering the polychromatic nature of x-rays used in the experiments, and the possible material differences between our digital ACR phantom model and the real ACR MAP phantom used in experiments.

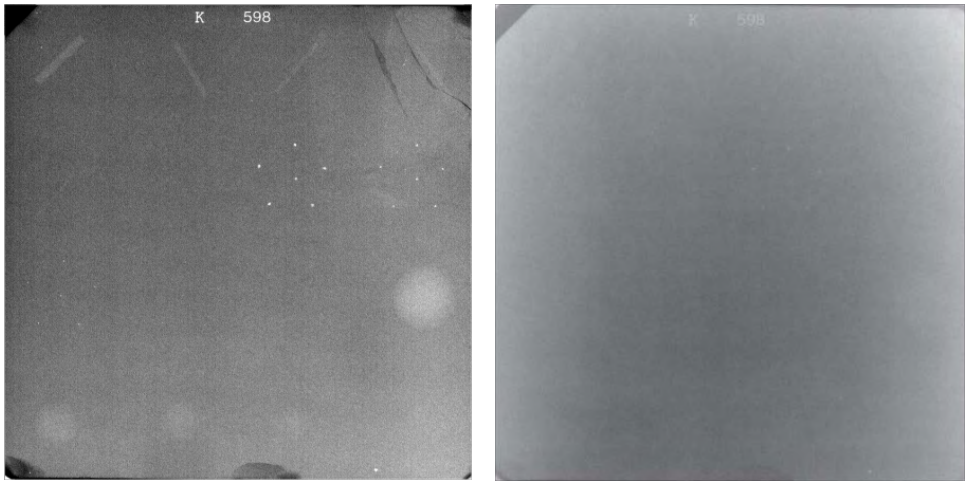

Fig. 4. Two images of a ACR accreditation phantom acquired with the 100 kVp and the same dose to phantom. (left) Phase contrast image of the phantom with M = 2. (right) Contact radiograph of the phantom.

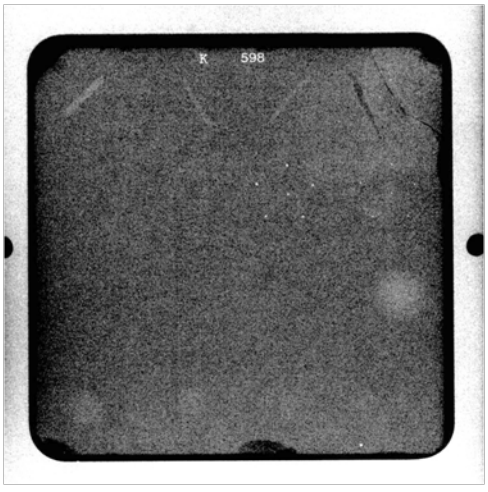

Fig. 5. A phase map of an ACR accreditation phantom retrieved by using the duality-based method from a single phase-sensitive projection. The projection was acquired with 120 kVp and an estimated average glandular dose of 98.9 mrad.

In summary, in this period we conducted phantom imaging studies with 100 kVp-140 kVp tube voltages and retrieved the phantom phase maps for fully exhibiting the phase contrast and providing quantitative

information on the phantom electron densities. The study shows that the high energy x-ray phase-sensitive projections combined with the duality-based phase retrieval method demonstrated the potential of enabling significant radiation reduction and quantification of tissue projective electron densities in future breast imaging applications.

Key Research Accomplishments

- The robustness of the phase retrieval methods is of critical importance for limiting and reducing radiation doses involved in x-ray phase imaging. In this period we have compared the AP-based phase retrieval method developed in the last period to the conventional TIE-based method by analyzing the phase maps retrieved from the experimental images of a phantom. We showed that in these experiments our AP-based method is to be superior to the TIE-based method for the robustness in performing the phase retrievals. This finding is of significance for developing future clinical applications of the x-ray phase imaging.

- Extending the research work on the phase retrieval methods, as a by-product of this project, we found a general formula to quantitatively relate the apparent linear attenuation coefficients to the sample's linear attenuation coefficients and refractive indices in the phase contrast tomography. This formula overcomes the gross inaccuracy of the existing formula in the literature in analyzing high-resolution phase contrast tomography, and it will be useful for correctly interpreting and quantifying the apparent linear attenuation coefficients in x-ray phase contrast tomography in the biomedical applications.

- In this period we conducted phantom imaging studies with 100 kVp -140 kVp tube voltages as is planned for developing low-dose and quantitative x-ray phase imaging techniques. In the phantom imaging we validated the optimal geometric configurations as determined in the first period based on the phase contrast visibility analysis. We performed the Monte Carlo simulations as well for accurately estimating the average glandular doses involved in the high-voltage imaging. In order to fully exhibit the phase contrast of phantom components and provide their projective electron densities, we performed a phase retrieval study to retrieve phantom phase maps by using a novel phase retrieval method that we developed. The results of the study show that the phase contrast exhibited in the retrieved phase maps compensates for the attenuation-contrast loss associated with using high tube-voltages, and with these techniques the radiation doses are reduced and quantitative information on phantom projective electron densities is obtained. These studies demonstrate that the techniques developed here has good potential of enabling significant radiation dose reduction and quantitative imaging with tissue electron density information in future breast imaging applications.

- **Reportable Outcomes**

In this project period we have published the research results in peer-reviewed journals and presented the work in national conferences, as listed in the following.

Peer-Reviewed Journal Article:

A. Yan, X. Wu, and H. Liu, Robustness of phase retrieval methods in x-ray phase contrast imaging: A comparison, Medical Physics 38: 5073-5080 (2011)

A. Yan, X. Wu, Apparent Linear Attenuation Coefficients in Phase Contrast X-Ray Tomography, Nuclear Instruments and Methods in Physics Research, B 269 1841-1843 (2011)

Published Abstract and Conference Presentation**:**

A. Yan, X. Wu, M. A. Yan, X. Wu, and H. Liu: Development of a prototype phase-sensitive x-ray breast imaging system", DoD Breast Cancer Research Program Era of Hope 2011 Conference, Aug. 3-Aug. 5, 2011, Orlando, Florida.

H. Liu H, X. Wu: Development and characterization of phase sensitive x- ray imaging systems, The 53rd Annual Meeting of the American Association of Physicists in Medicine, July 31-Aug. 4, 2011, Vancouver, Canada.

Conclusion

With the grant support by USAMRMC we have successfully conducted studies on x-ray phase imaging in the third period of this project. As the phase retrieval is a crucially important task of our project, in this period we have examined the robustness of phase retrieval methods against the projection image noises. In this period we compared the robustness of two phase-retrieval methods, as the common TIE-based method vs. the AP-based method that we developed, by analyzing the phase maps retrieved from the experimental images of a phantom. The comparison shows that the conventional TIE-based phase retrieval method is unstable against the noise in the wrap's projection images, while the AP-based method is shown in the experiment to be superior to the TIE-based method for the robustness in performing the phase retrieval. This finding is of importance for developing the phase imaging techniques.

In this period we made significant progress in developing low-dose and quantitative x-ray phase imaging. We have conducted phantom imaging studies with 100 kVp -140 kVp tube voltages and retrieved the phantom phase maps for fully exhibiting the phase contrast and providing quantitative information on the phantom electron densities. The results of the study show that the phase contrast exhibited in the retrieved phase maps compensates for the attenuation-contrast loss associated with using high tube-voltages, and with these techniques the radiation doses are reduced and quantitative information on phantom projective electron densities is obtained. These techniques developed in this period has good potential of enabling significant radiation dose reduction and quantitative imaging with tissue electron density information in future breast imaging applications.

In the next no-cost extension period, we will continue our research in developing low-dose and quantitative x-ray phase imaging with high energy x-rays. We plan to further optimize the design trade-off in the detector spatial resolutions and quantum efficiencies for achieving more large radiation dose reductions. We will refine our phase retrieval method for higher retrieval accuracies by better incorporating the x-ray spectral effects. These studies in next period will facilitate the development of the low dose quantitative phase imaging techniques for future breast imaging applications.

References:

Allen L, Oxley M. 2001. Phase retrieval from series of images obtained by defocus variation, Optics Communications 199: 65-75.

Wu, X., Liu, H. 2004. A new theory of phase-contrast x-ray imaging based on Wigner distributions. *Medical Physics* 31, 2378-2384.

Wu X, Liu, H, Yan, A. 2005. X-ray phase-attenuation duality and phase retrieval, Optics Letters 30: 379-381.

Yan A, Wu X, Liu H. 2008. An attenuation-partition based iterative phase retrieval algorithm for in-line phase-contrast imaging, Optics Express 16: 13330-13341.

Wu, X., Yan, A. 2009. Phase retrieval from one single phase contrast x-ray image, *Optics Express* 17, 11187-11196.

Yan A, Wu X, Liu H. 2010. Performance analysis of the attenuation-partition based iterative phase retrieval algorithm for in-line phase-contrast imaging, Optics Express 18: 16074-16089.

Yan A., Wu X. 2011. Apparent Linear Attenuation Coefficients in Phase Contrast X-Ray Tomography, Nuclear Instruments and Methods in Physics Research, B 269 1841-1843.

Yan A., Wu X., Liu H. 2011. Robustness of phase retrieval methods in x-ray phase contrast imaging: A comparison, Medical Physics 38: 5073-5080.

Appendices

Copies of following publications are enclosed for review.

Peer-Reviewed Journal Article**:**

A. Yan, X. Wu, and H. Liu, Robustness of phase retrieval methods in x-ray phase contrast imaging: A comparison, Medical Physics 38: 5073-5080 (2011)

A. Yan, X. Wu, Apparent Linear Attenuation Coefficients in Phase Contrast X-Ray Tomography, Nuclear Instruments and Methods in Physics Research, B 269 1841-1843 (2011)

Robustness of phase retrieval methods in x-ray phase contrast imaging: A comparison

Aimin Yan and Xizeng Wu[a)]
Department of Radiology, University of Alabama at Birmingham, Birmingham, Alabama 35233

Hong Liu
Center for Bioengineering and School of Electrical and Computer Engineering, University of Oklahoma, Norman, Oklahoma 73019

(Received 31 May 2011; revised 4 July 2011; accepted for publication 8 July 2011; published 17 August 2011)

Purpose: The robustness of the phase retrieval methods is of critical importance for limiting and reducing radiation doses involved in x-ray phase contrast imaging. This work is to compare the robustness of two phase retrieval methods by analyzing the phase maps retrieved from the experimental images of a phantom.
Methods: Two phase retrieval methods were compared. One method is based on the transport of intensity equation (TIE) for phase contrast projections, and the TIE-based method is the most commonly used method for phase retrieval in the literature. The other is the recently developed attenuation-partition based (AP-based) phase retrieval method. The authors applied these two methods to experimental projection images of an air-bubble wrap phantom for retrieving the phase map of the bubble wrap. The retrieved phase maps obtained by using the two methods are compared.
Results: In the wrap's phase map retrieved by using the TIE-based method, no bubble is recognizable, hence, this method failed completely for phase retrieval from these bubble wrap images. Even with the help of the Tikhonov regularization, the bubbles are still hardly visible and buried in the cluttered background in the retrieved phase map. The retrieved phase values with this method are grossly erroneous. In contrast, in the wrap's phase map retrieved by using the AP-based method, the bubbles are clearly recovered. The retrieved phase values with the AP-based method are reasonably close to the estimate based on the thickness-based measurement. The authors traced these stark performance differences of the two methods to their different techniques employed to deal with the singularity problem involved in the phase retrievals.
Conclusions: This comparison shows that the conventional TIE-based phase retrieval method, regardless if Tikhonov regularization is used or not, is unstable against the noise in the wrap's projection images, while the AP-based phase retrieval method is shown in these experiments to be superior to the TIE-based method for the robustness in performing the phase retrieval.
 [DOI: 10.1118/1.3618731]

Key words: x-ray imaging, phase contrast, phase retrieval

I. INTRODUCTION

In recent years, the in-line phase-contrast x-ray imaging has attracted intensive research efforts. The in-line phase-contrast x-ray imaging is a technique using the free space diffraction of phase-shifted x-rays to form the interference fringes at tissues' boundaries and interfaces in images.[1–8] In fact, for over 100 years, the tissue attenuation differences have been the sole contrast mechanism for medical x-ray imaging. However, when x-rays traverse the body parts, as a wave x-rays undergo phase shifts as well. The amount of the phase shift along an exit ray is determined by the tissue refractive indices along the ray. Note that x-ray refractive index n is a complex number and equal to $n = 1 - \delta + i\beta$, where δ is the refractive index decrement and responsible for x-ray phase shift, while β is the imaginary part of the refractive index and responsible for x-ray attenuation. The amount of x-ray phase shift along an exit ray is given by $\varphi = -(2\pi/\lambda)\int \delta ds$, where λ is the x-ray wavelength, and the integral is over the ray path.[1,2] In other words, the phase shift is equal to the projection of refractive index decrements scaled by a factor $(2\pi/\lambda)$. On the other hand, x-ray attenuation along an exit ray is determined by the projection of the tissue linear attenuation coefficients along the ray, which is equal to $(4\pi/\lambda)\int \beta ds$.[1,2] We have estimated δ and β values for the biological tissues and found that the tissue δ values $(10^{-6}$–$10^{-8})$ are about 1000 times greater than their β values $(10^{-9}$–$10^{-11})$ for 10–150 keV x-rays.[8] Hence, the differences in x-ray phase shifts between different tissues are about 1000 times greater than their differences in the projected linear attenuation coefficients. Therefore, the phase-contrast imaging techniques may greatly increase the lesion-detection sensitivity for x-ray imaging. The settings for the inline phase-sensitive imaging are similar to that of conventional x-ray imaging, provided a source with very small focal spot and a sufficiently large object-detector distance are required.[5,7,8] In the inline imaging setting, x-rays undergo phase shifts as traversing the imaged object, and then diffract

freely over a sufficiently large distance before reaching the detector. In this way, the tissues' phase contrast manifests as the dark-bright diffraction fringes at tissues' boundaries and interfaces in the measured images.[5,7,8] Hence, the inline phase contrast imaging has good potential of greatly enhancing the detection sensitivity and reducing radiation doses involved in the imaging.

However, as the interfaces and boundaries of the different tissue compartments are greatly accentuated in a phase-contrast image, the bulk phase contrast in a given tissue compartment, where the phase shifts may vary slowly, could get lost. This is because the phase contrast is proportional to the Laplacian and gradient differentials of the phase shifts, as is shown in Sec. II below. Moreover, the information about x-ray phase shifts are valuable for tissue characterizations, since x-ray phase shift along a ray is proportional to the projected tissue electron density, that is, $\varphi = -\lambda r_e \int \rho_e ds$, where r_e is the classic electron radius and ρ_e denotes the tissue electron density and the integral is over the ray path.[1,2] In order to fully exhibit tissue phase contrast and reconstruct tissue projected electron densities for quantitative tissue characterizations, one needs to extract the tissue phase shifts from the mixed contrast exhibited in a phase-sensitive projection. The procedure of retrieving the phase-shift map of an object from its phase-sensitive projections is called the phase retrieval.[10–14] A retrieved phase map is able to provide a quantitative map of the object's projected electron densities, which could be used for quantitative tissue characterizations.[12–14] Moreover, performing phase retrieval is necessary for reconstructing volumetric 3-D maps of tissue attenuation coefficients and refractive indices, respectively,[14,15] and for eliminating the phase-contrast caused artifacts in the volumetric 3-D images.[16]

Examining the robustness of phase retrieval methods against the projection noise, such as the x-ray photon quantum noise and others involved in the projection acquisitions, is an important task in phase contrast imaging. If a phase retrieval method is not robust against the noise, the method could become unstable and fail in phase retrievals if the acquired projection images had be contaminated with substantial noise. On the other hand, suppressing x-ray quantum noise may require using high radiation doses in the image acquisitions. For clinical applications, it is imperative to limit and reduce radiation doses involved, hence, it is critical to develop robust phase retrieval methods for future clinical applications of phase contrast imaging. The purpose of this work is to compare the robustness of two phase retrieval methods by means of analyzing the phase maps retrieved from the experimental projection images of an air-bubble wrap phantom. We will first introduce the phase retrieval method that is based on the transport of intensity equation (TIE), which describes how the phase contrast is encoded in the projection images.[10,11] This TIE-based method is the most commonly used method for phase retrieval in the literature. We will then introduce a recently developed phase retrieval method, namely the attenuation-partition based (AP-based) method.[13] In order to examine the robustness of these two methods against noises, we applied these two phase retrieval methods to experimental phantom images, namely a radiograph and a phase contrast image of the air-bubble wrap phantom, for the phase retrievals. We will analyze the retrieved phase maps obtained by using the two methods and compare their performances in the robustness against noises in the phantom images. In Sec. IV, we explain that these performance differences of the two phase retrieval methods are rooted in their different techniques employed to deal with the singularity problem involved in the phase retrievals. In addition, other factors that may affect the phase retrieval performance will be briefly discussed as well.

II. PHASE RETRIEVAL METHODS

In phase contrast images, the attenuation contrast and phase contrast are mixed together. In order to retrieve phase maps from phase contrast projection images, one should understand how the phase contrast is encoded in the projection images. This understanding can be gained from the x-ray propagation equation such as the TIE.[10,11] This equation can be derived either from the x-ray Fresnel-diffraction equation or the Wigner distribution based phase-space formalism.[9–11] If we denote the x-ray transmission image of an object, or equivalently its x-ray attenuation map by $A_o^2(\vec{r})$ and the x-ray phase-shift map of the object by $\varphi(\vec{r})$, then the detected x-ray intensities are given by[8,11,17]

$$I(\vec{r}_D) = \frac{I_{in}}{M^2}\left\{A_o^2(\vec{r}_D/M) - \frac{R_2\bar{\lambda}}{2\pi M}\nabla\cdot(A_o^2(\vec{r}_D/M)\nabla_\varphi(\vec{r}_D/M))\right\} \quad (1)$$

where $\bar{\lambda}$ is the average x-ray wavelength of the polychromatic x-rays. In Eq. (1), I_{in} is the entrance x-ray intensity, R_1 is the source-object distance set in the projection, R_2 is the object-detector distance, $M = (R_1 + R_2)/R_1$, the magnification factor in the projection, and $\vec{r}_D$ denotes the position vector in the detector plane. In Eq. (1), the operator ∇ denotes the two-dimensional transverse gradient differential operator. For the purpose of this work, we assume that the x-ray source's focus spot is ideally point-like and the detector employed is an ideal detector. Obviously, the detected x-ray intensity $I(\vec{r}_D)$ is determined not only by attenuation map $A_o^2(\vec{r})$ in the projection, but also by the encoded phase contrast, that is, by the transverse Laplacian and gradient differentials of the phase-shift map $\varphi(\vec{r})$ in the projection. Since the phase contrast and attenuation contrast are mixed together in a phase contrast image, as is shown by Eq. (1), hence measuring a single phase-contrast image is not enough for retrieving the phase-shift map $\varphi(\vec{r})$ in the projection. Therefore, in general, at least two projection images are needed for retrieving the phase-shift map $\varphi(\vec{r})$ of the object.

The most commonly used phase retrieval method in the literature is the TIE-based method. In this method, two acquired projection images of an object are used for retrieving the phase-shift map of the object: one is a contact radiograph $A_o^2(\vec{r})$ of the object, the other is a phase contrast projection image $I(\vec{r}_D)$ of the object. One then is able to retrieve the phase-shift map $\varphi(\vec{r})$ by solving Eq. (1) for $\varphi(\vec{r})$ as follows[12]:

$$\varphi(\vec{r}) = -\left(2\pi M/\bar{\lambda}R_2\right)\nabla^{-2} \times \left\{\nabla\cdot\left[\frac{1}{A_o^2}\nabla\left(\nabla^{-2}\left(\frac{M^2 I}{I_{in}} - A_o^2\right)\right)\right]\right\}. \quad (2)$$

In above equation, the operator ∇^{-2} denotes the inverse of the Laplacian differential operator $\nabla^2 \equiv (\partial^2/\partial x^2 + \partial^2/\partial y^2)$. The inverse Laplacian operator ∇^{-2} is a pseudodifferential operator. The action on a function $g(\vec{r})$ of a pseudodifferential operator such as ∇^{-2} is defined as

$$\nabla^{-2} g(\vec{r}) \equiv \iint \exp(i2\pi(\vec{s}-\vec{r})\cdot\vec{f})\cdot\left(-1/\left(4\pi^2\vec{f}^2\right)\right) \times g(\vec{s})d^2\vec{s}\cdot d^2\vec{f}. \quad (3)$$

In Eq. (3), $\vec{s}$ and $\vec{f}$ denote the integral variables in the coordinate space and frequency space, respectively. Hence, one can compute the phase map $\varphi(\vec{r})$ by using Eq. (2) with the help of Eq. (3). The TIE-based method is effective and fast for phase retrievals in the cases with strong phase contrast effects and low noise levels as is shown in many cases discussed in the literature.[11,12] However, the Achilles heel of the TIE-based method lies at the inverse Laplacian operator ∇^{-2} involved in Eq. (2). The operator ∇^{-2} adds a zero-frequency singularity to Eq. (2), as is suggested by Eq. (3). As we will see below, the singularity may amplify the noise randomly embedded in the acquired images and result in instability in phase retrievals.

In order to get rid of the singular pseudodifferential operator ∇^{-2} involved in the TIE-based phase retrievals, we recently developed a novel phase retrieval method: the AP based method or the AP-based method for short.[13,18] Our idea in this method is to utilize the correlation between the x-ray phase shift and its attenuation to eliminate any singularity involved in the phase retrievals. As is well known, in the diagnostic x-ray imaging, x-ray attenuation A_o^2 arises from three x-ray-matter interactions: the photoelectric absorption, the coherent scattering, and the incoherent scattering. Correspondingly, we can partition the x-ray attenuation into two parts: the Compton scattering-caused attenuation A_{KN}^2 and the attenuation caused by photoelectric absorption and coherent scattering, which is denoted by $A_{pe,coh}^2(\vec{r})$. That is, we can partition the overall x-ray attenuation A_o^2 into a product of two parts

$$A_o^2(\vec{r}) = A_{KN}^2(\vec{r})\cdot A_{pe,coh}^2(\vec{r}). \quad (4)$$

The reason of factoring out A_{KN}^2 is that both of A_{KN}^2 and the phase-shift φ are determined by the tissue's electron density

$$A_{KN}(\vec{r}) = \exp\left[-\frac{\bar{\sigma}_{KN}}{2}\rho_{e,p}(\vec{r})\right], \quad \varphi(\vec{r}) = -\bar{\lambda}r_e\rho_{e,p}(\vec{r}) \quad (5)$$

where $r_e = 2.818\times10^{-15}$ m is the classical electron radius, $\rho_{e,p}$, the projected electron density along the ray path, that is, $\rho_{e,p}(\vec{r}) = \int_{ray}\rho_e(\vec{r},z)dz$, and $\bar{\sigma}_{KN}$ denotes the average Compton scattering cross-section for polychromatic x-rays. Note that Compton scattering cross-section is given by the Klein-Nishina total cross-section[19]

$$\sigma_{KN}(E) = 2\pi r_e^2\left\{\frac{1+\eta}{\eta^2}\left[\frac{2(1+\eta)}{1+2\eta} - \frac{1}{\eta}\log(1+2\eta)\right] + \frac{1}{2\eta}\log(1+2\eta) - \frac{1+3\eta}{(1+2\eta)^2}\right\}, \quad (6)$$

where $\eta \equiv E\ /511$ keV and it slowly varies with x-ray energy E for $E \ll 511$ keV. We observed that the extent of the correlation between phase and attenuation depends on the x-ray photon energies and the tissues elemental compositions. For example, for light elements with atomic numbers $Z < 10$ and x-rays of 60 keV or higher, the x-ray-matter interactions are dominated by the Compton scattering, hence, both the tissue attenuation and phase shift are all determined by tissues' electron density distributions. We call this relationship between phase shift and attenuation the phase-attenuation duality, and we define the so-called duality transform as[20]

$$\mathfrak{D}(I(\vec{r}_D)) \equiv \left(1 - \left(\bar{\lambda}^2 R_2 r_e/2\pi M\bar{\sigma}_{KN}\right)\nabla^2\right)^{-1}\cdot\left(\frac{M^2 I(\vec{r}_D)}{I_{IN}}\right). \quad (7)$$

For the cases where the x-ray-matter interactions are dominated by the Compton scattering, we proved that the attenuation A_{KN}^2 can be found from a single phase contrast image $I(\vec{r}_D)$ by means of the duality transform such that $A_{KN}^2(\vec{r}) = \mathfrak{D}(I(\vec{r}_D))$.[20] With the help of the phase-attenuation duality, the phase-shift map of the object can be simply retrieved as

$$\varphi(\vec{r}) = \frac{\bar{\lambda}r_e}{\bar{\sigma}_{KN}}\ln A_{KN}^2(\vec{r}) = \frac{\bar{\lambda}r_e}{\bar{\sigma}_{KN}}\ln\mathfrak{D}(I(\vec{r}_D)). \quad (8)$$

We call this formula as the phase-attenuation duality-based phase retrieval formula.[20] One significant advantage of this duality-based phase retrieval formula is that the pseudodifferential operator $\left(1 - \left(\bar{\lambda}^2 R_2 r_e/2\pi M\bar{\sigma}_{KN}\right)\nabla^2\right)^{-1}$ involved in Eqs. (7) and (8) is free of any singularity. Therefore, the phase retrieval method based on the phase-attenuation duality is stable and robust against the noise in images.[20]

Unfortunately, the phase-attenuation duality does not hold in some other cases such as imaging with low energy x-rays or imaging bones and calcifications that contain substantial amount of heavy elements. In those cases, the retrieved phase map using Eq. (8) may provide merely coarse estimates of the real phase maps of the imaged objects. In order to overcome this limitation of the duality-based phase retrieval formula Eq. (8), recently we proposed to correct the errors iteratively through repeated comparisons of the computed estimates of the x-ray Fresnel-diffraction intensities against the acquired projection intensities. To implement this strategy, we developed the attenuation-partition based iterative algorithm, whose flow chart is shown in Fig. 1.[13] While interested readers can find the mathematical proofs of the algorithm in Ref. 13, here, we give a brief explanation of this algorithm flow chart in Fig. 1. In this flow chart, A_o^2 denotes the attenuation map of the imaged object measured from its contact radiograph and I is the acquired phase contrast image of the object. In the flow chart, I_{KN} denotes the simulated phase contrast image formed

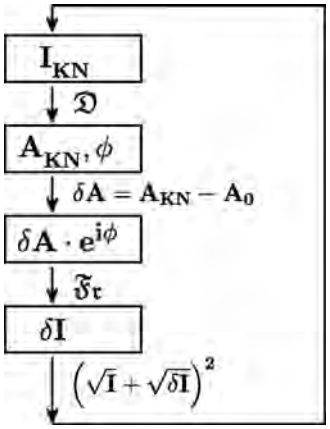

FIG. 1. Flow chart of the AP based iterative algorithm.

by using the estimated object's electron densities and by turning off the attenuation processes associated with x-ray photoelectric absorption and coherent scattering. In Fig. 1, two transforms are implemented in the iterations, one is the Fresnel-diffraction transform $\mathfrak{F}_{re}$, which implements x-ray Fresnel-diffraction,[21] and the other is the duality transform $\mathfrak{D}$ as is defined in Eq. (7). According to this flow chart (Fig. 1) of the AP-based phase retrieval method, one first applies the duality transform $\mathfrak{D}$ to the acquired phase contrast image I to obtain an estimate of A_{KN}^2 and the phase map φ of the object. One then compares A_{KN}^2 against the measured A_o^2 and computes the error $\delta A \equiv A_{KN} - A_0$. Applying the Fresnel-diffraction transform $\mathfrak{F}_{re}$ to the fictitious transmission function $\delta A \cdot \exp(i\varphi)$, one computes the I_{KN} -correction $\delta I \equiv \left|\mathfrak{F}_{re}(\delta A \cdot \exp(i\varphi))\right|^2$, and a new estimate of I_{KN} is determined as $I_{KN} = (\sqrt{I} + \sqrt{\delta I})^2$. With this new estimate of I_{KN}, one can start a new round of the iteration as is indicated in the flow chart Fig. 1. The iteration converges when the I_{KN} does not change substantially with further iteration steps.[13]

III. COMPARISON OF THE TWO PHASE RETRIEVAL METHODS

In order to compare the robustness of above two phase retrieval methods, namely, the TIE-based method and the AP-based method, we applied the two methods for retrieving the phase map of a piece of air-bubble wrap. In the bubble wrap, the air packets are locked between two thin layers of low-density polyethylene films forming the air bubbles. Shown in Fig. 2(a) is a contact radiograph of the wrap. The x-ray source used was a micro-focus x-ray tube (L8121-02, Hamamatsu) with a focal spot size of 7 μm. The source has a tungsten target without added filtration and was operating at 40 kVp and 0.2 mA for a 30 s exposure. The average x-ray photon energy was estimated at 14.6 keV for the 40 kVp x-rays. In this acquisition, the source-detector distance (SID) was set to 1.78 m. The imaging detector employed was an aSe-based flat-panel detector (DirectRay, Hologic) with a pixel pitch of 140 μm. Since the thin polyethylene films and locked air bubbles in the wrap generate little differences in x-ray attenuation, hence, the wrap's radiograph in Fig. 2(a) exhibits only little image contrast, and the x-ray quantum noise in the acquisition

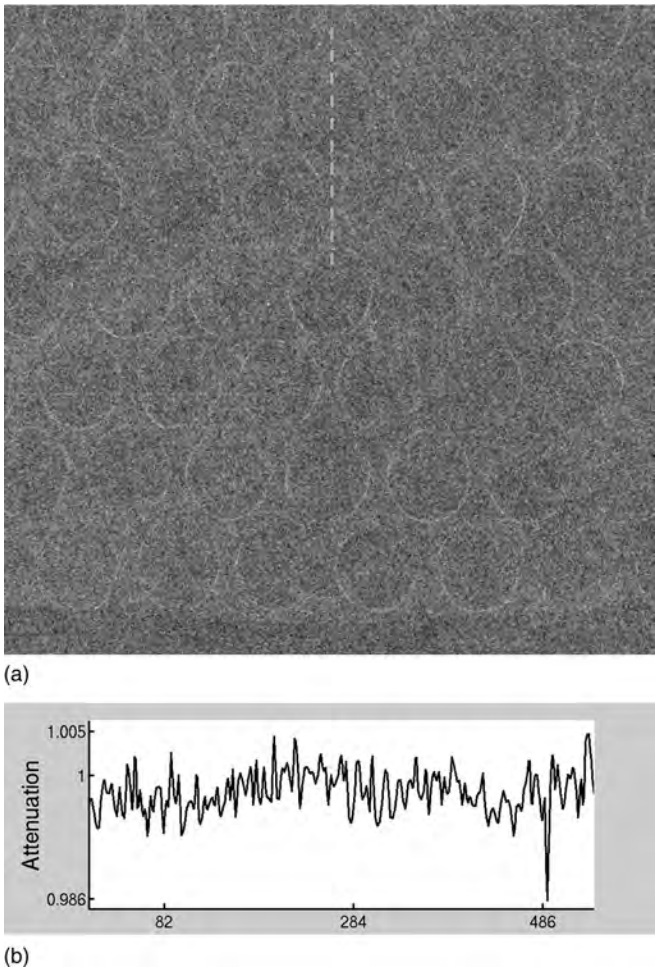

FIG. 2. (a) Contact radiograph of the bubble wrap acquired at 40 kVp and with a SID = 1.75 m. (b) Intensity profile along the marked line on (a).

masked the wrap's details such that the rims of many bubbles are not visible on the image. Figure 2(b) shows a profile of image intensities along the marked dash line on Fig. 2(a) and the profile reveals how the noisy intensity variations mask the low contrast rims of the bubbles. In contrast, Fig. 3(a) is a phase contrast image of the bubble wrap. This phase contrast image was acquired with a sample-detector distance $R_2 = 1.15$ m and otherwise the same technique settings as that used for the radiograph, that is, with the same focal spot size, same tube voltage, same tube current and exposure time, same SID, and the same detector. However, in this projection, the phase-shifted x-rays were allowed to freely diffract over 1.15-m long distance on their way to the detector and to form the interference fringes at the bubble boundaries on the image. As is shown in Fig. 3(a), the phase contrast depicts not only the bubble rims, but also the dents inside the bubble domes. The enhancement is resulted from the rapid changes of the projected thicknesses of the polyethylene films at the bubble rims and the dents inside bubble domes. These rapid changes in the projected thicknesses of polyethylene generate as well rapid changes in x-ray phase shifts, since the x-ray phase shifts are given by $\varphi(\vec{r}) = -\lambda r_e \rho_e T_p(\vec{r})$, where ρ_e denotes polyethylene film's electron density and $T_p(\vec{r})$ denotes projected thickness of polyethylene along the ray. According to

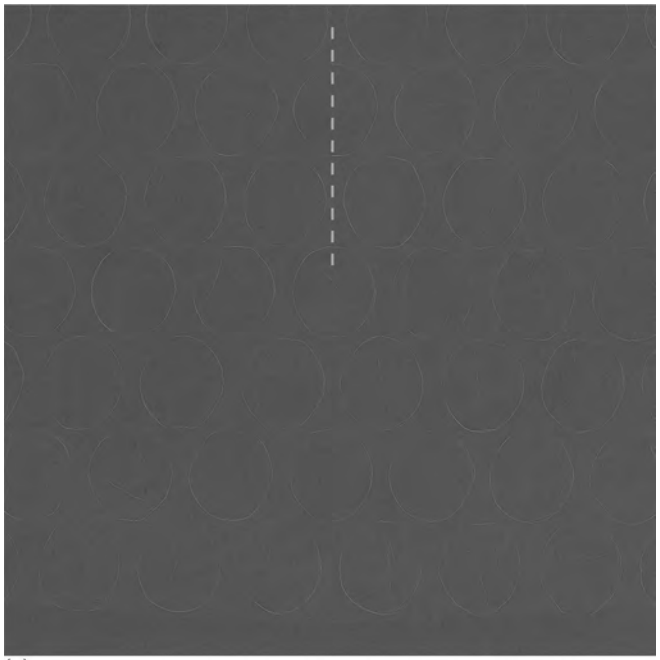

FIG. 3. (a) Phase contrast image of the bubble wrap, which was acquired at 40 kVp and with a SID = 1.75 m and a magnification factor M = 2.8. (b) Intensity profile along the marked line on Fig. 3(a).

Eq. (1), the Laplacian and gradient differentials of the rapid phase shifts generated large x-ray intensity variations, which manifest as the bright-dark fringes flank along the bubble rims in Fig. 3(a). Figure 3(b) shows a profile of image intensities along the marked dash line on Fig. 3(a), as the line traces the same positions as indicated by the dash line on Fig. 2(a). The downward and upward overshooting of the intensity values in the profile represent the bright and dark fringes at the bubble boundaries in phase contrast image Fig. 3(a). These up-down bipolar overshootings of intensities are much larger than the background noise, hence, the noise gets masked in Fig. 3(a). While the edge-enhancement generated by phase-contrast is generally useful for imaging the wrap, however, such edge-enhancements may lead interpretation errors in the characterization of the wrap's structure and composition. For example, in Fig. 3(a), the dark fringes flanked the enhanced bubble rims may be confused with possible structural breaks in the wrap sample, although we knew in advance that this wrap sample is free of any damage. In order to fully exhibit the wrap's phase contrast and correctly characterize the bubble wrap, it is necessary to perform the phase retrieval. In order to retrieve the wrap's phase-shift map from the wrap's radiograph [Fig. 2(a)] and its phase contrast image [Fig. 3(a)], we first employed the TIE-based phase retrieval formula Eq. (2). The retrieved phase map with the TIE-method is shown Fig. 4(a). Apparently, the phase retrieval failed completely, since no bubble is recognizable in Fig. 4(a). Although the failure can be

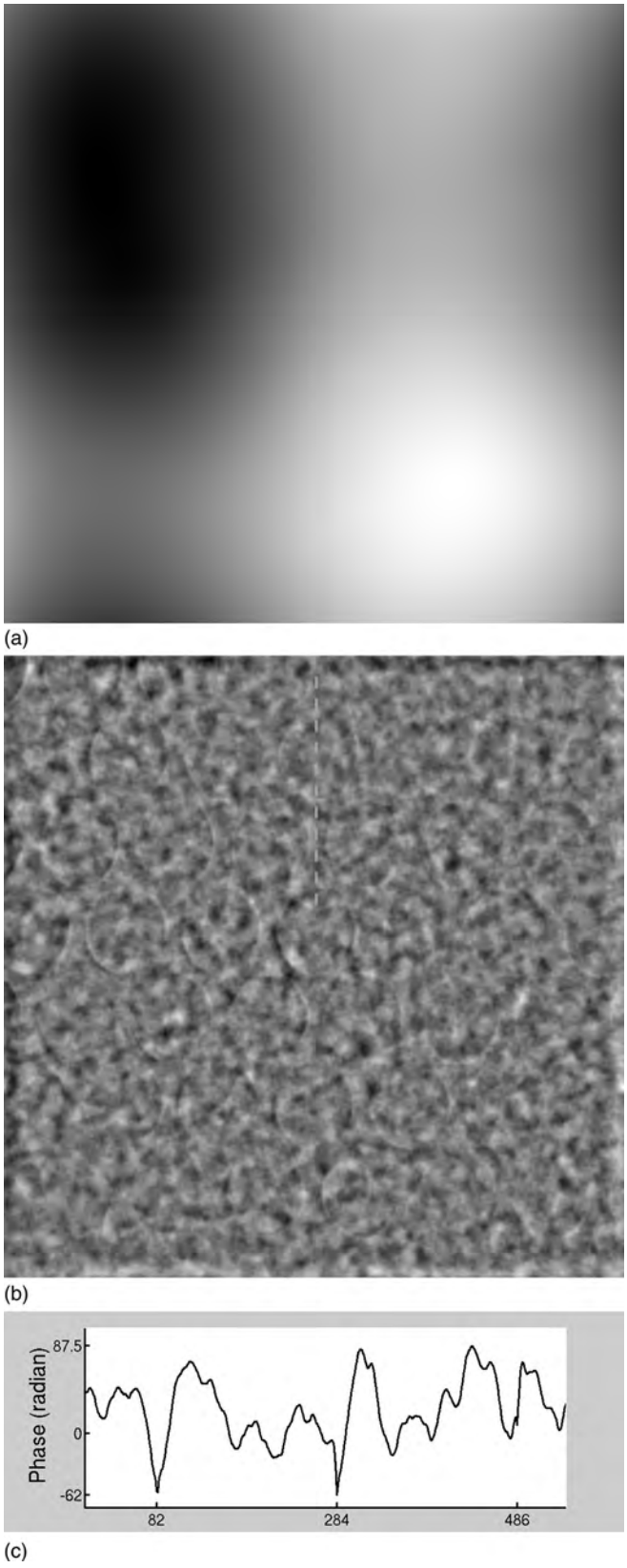

FIG. 4. Retrieved phase maps of the bubble wrap. (a) With the TIE-based method. (b) With the TIE-based method and Tikhonov regularization. (c) Profile of the retrieved phase values along the marked line on (b).

ascribed to the high-levels of the quantum noise presented in the radiograph of Fig. 2(a), but it is rooted in the intrinsic instability of the TIE-method. As we pointed out in Sec. II, the inverse Laplacian operator ∇^{-2} plugs in the zero-frequency singularity into the TIE-base phase retrieval formula Eq. (2). The singularity amplified the noise randomly embedded in the projections and results in the failure in the phase retrievals. To mend the instability of the TIE-method, one can try to apply the regularization techniques to tame the singularity-caused problems. A common regularization technique in the literature is Tikhonov regularization.[22] With this regularization scheme, one replaces the inverse Laplacian operator ∇^{-2} by a pseudodifferential operator $\nabla^2/[(\nabla^2)^2+\alpha^2]$, where α is the regularization parameter, which is roughly proportional to the images noise-signal ratios of the images.[22] In essence, Tikhonov regularization seeks the minimum-norm, least squares solution of Eq. (2). While the Tikhonov regularization of the inverse Laplacian operator may tame the instability, it sacrifices the phase retrieval accuracies. The performance in phase retrieval of Tikhonov regularization is highly dependent on the amounts of noise presented in the images. The regularization parameter α was selected through a trial by comparing the phase maps retrieved with a wide range of α-values such as $\alpha=\Delta u^2$, $5\,\Delta u^2$, $10\,\Delta u^2$, $50\,\Delta u^2$, $100\,\Delta u^2$, $200\,\Delta u^2$, $300\,\Delta u^2$, and $500\,\Delta u^2$, where Δu is the frequency sampling-step used in the phase retrieval. Figure 4(b) is the wrap phase map retrieved using the TIE-method and Tikhonov regularization with $\alpha=200$ and $\Delta u^2=3.782\times10^{-8}\,\mu\text{m}^{-2}$, which was the α -value for the best results as determined from the trial. Apparently, these retrieval results are very unsatisfactory. In Fig. 4(b), the bubble rims are hardly visible in the extremely cluttered background. Figure 4(c) shows the profile of the retrieved phase values along the marked dash line on Fig. 4(b). As we will explain below that these phase values are grossly erroneous.

As a comparison, we have applied the AP-based method to the wrap's images in Figs. 2(a) and 3(a) for the phase retrieval as well. Following the method's iteration flow chart in Fig. 1, we succeeded in retrieving the wrap's phase map of the bubble wrap with ten iteration steps. Figure 5(a) is the retrieved phase map of the wrap with the AP-based method. In a stark contrast to Figs. 4(a) and 4(b) where the bubble rims are hardly visible, the bubble rims are prominently depicted in Fig. 5(a). A profile of retrieved phase values along the marked line on Fig. 5(a) is shown in Fig. 5(b). Note that all the marked lines in Figs. 3(a), 4(b), and 5(a), respectively correspond to the same line defined on the bubble wrap. In this way, one can easily compare the three profiles shown in Figs. 3(b), 4(c), and 5(b). In order to study the quantitative aspects of the retrieved phase maps of the wrap, remember that the amount of phase shift along a ray is given by $\varphi(\vec{r})=-\lambda r_e\rho_e T_e(\vec{r})$, here, ρ_e denotes polyethylene film's electron density and $T_p(\vec{r})$ denotes projected thickness of polyethylene along the ray. Note that x-ray phase shifts should be of negative values, as x-ray refractive indices of tissues and materials are complex and their real part are less than one. The x-rays traversed longer paths in polyethylene at the bubble rims and incurred larger phase shifts, as

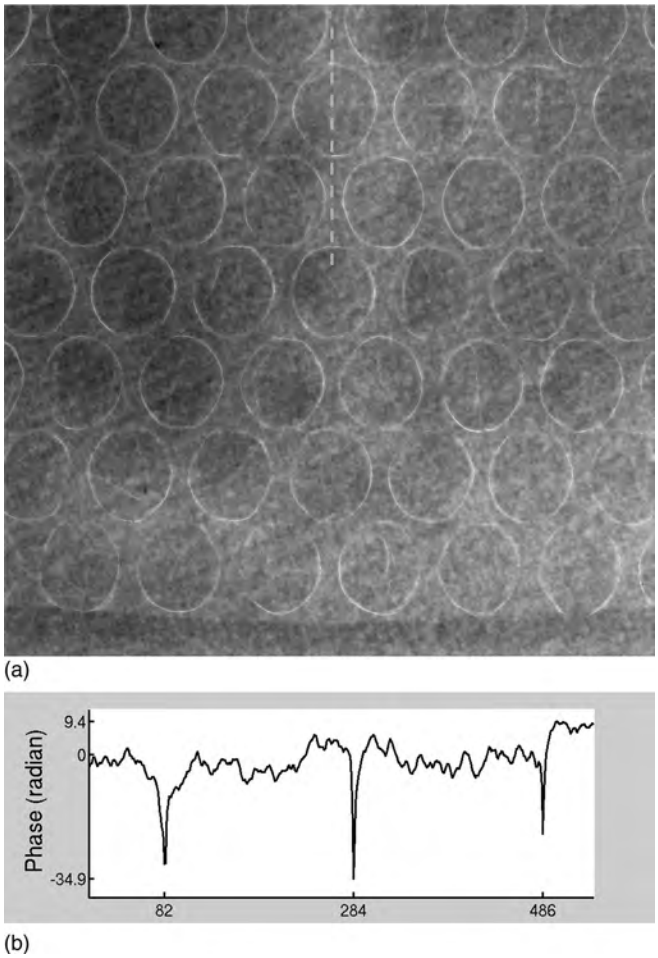

FIG. 5. (a) Retrieved phase maps of the bubble wrap with the AP-based method. (b) Profile of the retrieved phase values along the marked line on (a).

compared to other parts of the wrap. For example, the three sharp negative peaks in the profile Fig. 5(b) reflect the large x-ray phase shifts incurred at the three rim locations along the marked line in Fig. 5(a). In order to gauge the accuracies of the retrieved phase values profiled in Fig. 5(b), one has to know the values of $T_p(\vec{r})$, the projected thicknesses in polyethylene films. Apparently, $T_p(\vec{r})$ depends on the local curvatures of bubble domes and the incident angles of the rays. While it is hard to measure $T_p(\vec{r})$ values in the bubbles, we measured the thicknesses of the flat bases between bubbles using a caliber ruler, and we found that the base thickness was about 0.055 mm. Knowing that the molecular formula of the low-density polyethylene film is $(C_2H_4)_n$ and its mass density is $0.925\ \text{g/cm}^3$, we calculated its electron density as $3.18\times10^{23}/\text{cm}^3$. Assuming approximately all rays have normal incidence, we find that the approximate phase shifts at the flat bases between bubbles is about -4.2 radian. On the other hand, according to the phase profile in Fig. 5(b), the average phase shift at the flat bases between bubbles is -1.05 radian. Obviously, these two estimates of the phase values though different, but are reasonably close. In comparison, the phase profile in Fig. 4(c), which was obtained by using the TIE-based method with Tikhonov regularization, depicts just messy up-down peaks buried in cluttered and

noisy background. In the phase profile, Fig. 4(c) only two negative peaks at the rims are barely recognizable, and the third expected negative peak completely disappears. According to this profile, the phase-shift values at the bases fluctuate over a wide range from 0 to +87.5 radian with an average of +27.3 radian, while x-ray phase shifts should be negative. Hence, the average phase value of flat bases estimated based on the profile, Fig. 4(c) is in a gross discrepancy with the thickness measurement-based estimate. Therefore, the above comparisons show clearly that the AP-based phase retrieval method is shown to be superior to the TIE-based method, regardless if the Tikhonov regularization is used, in performing the phase retrieval for the bubble wrap.

Before ending this section, we want to demonstrate the usefulness of performing the phase retrieval for tissue and material characterizations by comparing the bubble wrap's phase map in Fig. 5(a) to its phase contrast image in Fig. 3(a). As we pointed out earlier, the dark fringes which are flanking the bubble rims in the phase contrast image Fig. 3(a), may be confused for indicating possible structural breaks in the bubble wrap. In contrast to Fig. 3(a) riddled with the dark fringes, the retrieved phase map Fig. 5(a) does not present any dark fringes at all. This observation is also verified by comparing the phase profile Fig. 5(b) to the intensity profile Fig. 3(b). The up-down bipolar overshootings appearing in Fig. 3(b) disappear in the phase profile Fig. 5(b), where only sharp downward peaks present for depicting the large phase shifts at the bubble rims. Therefore, the wrap's phase map Fig. 5(a) clarifies the nature of the dark fringes in Fig. 3(a) such that these dark fringes do not indicate any structural break in the wrap sample.

IV. DISCUSSION AND CONCLUSIONS

This study demonstrates that the robustness against noises of a phase retrieval method is critical for the qualities of the retrieved phase map. Specifically, the striking differences between the retrieved phase maps in Figs. 4(a) and 4(b), and Fig. 5(a) underline the importance of removing the zero-frequency singularity that is intrinsic to the TIE-based method. While the TIE-based phase retrieval method is computational effective for the cases with strong phase contrast effects and low noise levels,[11,12] it completely failed in retrieving the phase map of the bubble wrap, as is shown in Figs. 4(a) and 4(b). This is because the noise problem is especially challenging for the case at hand, as the bubble wrap has very low attenuation contrast and only moderate x-ray exposures were applied in bubble image acquisitions. From mathematical viewpoint, the TIE-based phase retrieval formula Eq. (2) is ill-posed, since it involves the inverse Laplacian operator ∇^{-2} that owns a zero-frequency singularity. Beyond the mathematics formality, this zero-frequency singularity reflects the fact that the phase contrast projection is insensitive to the slow variations of x-ray phase shifts. Seeking to recover the phase shifts by comparing the two projection images contaminated with noise, the TIE-based method has amplified the noise in retrieving the slowly varying phase shifts and ruined the phase retrieval completely. The Tikhonov regularization mends the singularity problem by replacing the inverse Laplacian operator ∇^{-2} in Eq. (2) by a pseudodifferential operator $\nabla^2/[(\nabla^2)^2+\alpha^2]$ with a regularization parameter $\alpha^2 > 0$. As is shown in Fig. 4(b), this regularization made some but only little improvement compared to Fig. 4(a) as the bubbles start to appear in the phase map but are still hardly visible. From the mathematical formulation of the Tikhonov regularization technique, it is clear that Tikhonov regularization just limits the overall magnitude of the errors caused by the noise in the retrieved phase map, but the details of the original phase map could still get lost in the retrieval.[22] The AP-based method mends the singularity problem by utilizing the correlations between x-ray attenuation and x-ray phase shifts generated by tissues or materials, as is shown in Eq. (8). In a sense, the AP-based method utilizes the object's x-ray attenuation to get rid of the low-frequency singularity and the associated noise amplification. This physics-motivated regularization scheme for the AP-based method is expected to be more effective than Tikhonov regularization in phase retrievals. The greatly improved quality of the retrieved phase map shown in Fig. 5(a), as compared to Figs. 4(a) and 4(b), validates this expectation. Hence, the performance differences of these phase retrieval methods underscore the importance of developing an effective method to remove the singularity that is intrinsic to the TIE-based method. After all, the high noise levels in the acquired images still take tolls on the quality of the phase map Fig. 5(a) retrieved the AP-method, where the noise are quite visible. While increasing radiation doses used in the projections is a possible solution for improving phase retrievals, but the radiation dose constraints are stringent in many applications. In clinical applications, it is imperative to limit and reduce radiation doses involved in the imaging. Therefore, more research is needed for developing ever-improved phase retrieval methods for future clinical applications of phase contrast imaging.

Other factors, which are less critical to the robustness of phase retrieval but may affect the accuracies of retrieved phase maps, include the detector calibrations such as the flat-field and gain corrections, and the ways to incorporate the spectral averaging effects of polychromatic x-rays. In fact, the residual background nonuniformity in the acquired images [Figs. 2(a) and 3(a)] also caused variations in the background phase values in Fig. 5 and reduced their accuracies. A careful detector calibration in future experiments should avoid this kind of problem. In addition, note that x-ray wavelength enters as an important parameter in Eq. (2) for the TIE-based method, and in the flow chart in Fig. 1 for the AP-based method. The average x-ray wavelength used in the phase retrievals should represent the wavelength's linear and nonliner effects averaged over the exiting x-rays spectrum and the detector's spectral response. For the TIE-based method, several works discussed the ways of performing the spectral averages over polychromatic x-rays.[8,23] We did not use these techniques in this work, because the TIE-based method in any way failed the wrap's phase retrieval. In this work, we simply use the estimated average photon energy of the incident x-ray to incorporating the spectral averaging. In the future, we may develop more elaborated ways for incorporating the spectral averaging effects. Finally, we mention that one could as well employ a special phase retrieval method for the simple samples such as the bubble wrap. This

special method works specifically for the single-material homogeneous samples, as long as the linear attenuation coefficient and refractive index of this material are provided. In this special method, the phase map of a single-material sample can be retrieved from just a single phase contrast image of the sample.[24] The air-bubble wrap can be approximately treated as a single-material sample as the air in bubbles contributes negligibly to x-ray attenuation and phase shifts. In this work, we do not compare this special method for single-material samples to the TIE-based and AP-based methods, since both the TIE-based and AP-based methods are the general phase retrieval methods applicable for any general objects of inhomogeneous materials.

In summary, in this work, we compared the robustness of two phase retrieval methods, the TIE-based method and the AP-based method, by analyzing the retrieved phase maps from the experimental projection images of an air-bubble wrap. We showed that the TIE-based method, regardless if the Tikhonov regularization is used, failed in retrieving the wrap's phase map. In contrast, in the wrap phase map retrieved by using the AP-based method bubbles are clearly recovered. The retrieved phase values with this method are reasonably close to the estimate based on the thickness-based measurement. The stark performance differences of the two methods are rooted in their different techniques employed to deal with the singularity problem. This comparison shows that the conventional TIE-based phase retrieval method, regardless of using Tikhonov regularization or not, is unstable against the noise in the wrap's projection images, while the AP-based phase retrieval method is shown in these experiments to be superior to the TIE-based method for the robustness in performing the phase retrieval.

ACKNOWLEDGMENTS

This research was supported in part by the Department of Defense Breast Cancer Research Program under Award No. W81XWH-08-1-0613 and the NIH Grant No. R01CA142587. H. Liu would like to acknowledge the support of Charles and Jean Smith Chair endowment fund as well.

[a]Author to whom correspondence should be addressed. Electronic mail: xwu@uabmc.edu

[1]A. Snigirev *et al.*, "On the possibilities of x-ray phase contrast microimaging by coherent high-energy synchrotron radiation," Rev. Sci. Instrum. **66**, 5486–5492 (1995).
[2]S. Wilkins, T. Gureyev, D. Gao, A. Pogany, and A. Stevenson, "Phase contrast imaging using polychromatic hard x-ray," Nature **384**, 335–338 (1996).
[3]A. Pogany, D. Gao, and S. Wilkins, "Contrast and resolution in imaging with a microfocus x-ray source," Rev. Sci. Instrum. **68**, 2774–2782 (1997).
[4]P. Cloetens, R. Barrett, J. Baruchel, J.-P. Guigay, and M. Schlenker, "Phase objects in synchrotron radiation hard X-ray imaging," J. Phys. D: Appl. Phys. **29**, 133–146 (1996).
[5]C. J. Kotre and I. P. Birch, "Phase contrast enhancement of x-ray mammography: A design study," Phys. Med. Biol. **44**, 2853–2866 (1999).
[6]F. Arfelli *et al.*, "Mammography with synchrotron radiation: Phase-detected Techniques," Radiology **215**, 286–293 (2000).
[7]E. Donnelly and R. Price, "Effect of kVp on edge-enhancement index in phase-contrast radiography," Med. Phy. **29**, 999–1002 (2002).
[8]X. Wu and H. Liu, "Clinical implementation of phase contrast x-ray imaging: Theoretical foundation and design considerations," Med. Phys. **30**, 2169–2179 (2003).
[9]X. Wu and H. Liu, "A new theory of phase-contrast x-ray imaging based on Wigner distributions," Med. Phys. **31**, 2378–2384, (2004).
[10]M. Teague, "Deterministic phase retrieval: a Green's function solution," J. Opt. Soc. Am. **73**, 1434–1441 (1983).
[11]K. Nugent, T. Gureyev, D. Cookson, D. Paganin, and Z. Barnea, "Quantitative phase imaging using hard x rays," Phys. Rev. Lett. **77**, 2961–2965 (1996).
[12]L. Allen and M. Oxley, "Phase retrieval from series of images obtained by defocus variation," Opt. Commun. **199**, 65–85 (2001).
[13]A. Yan, X. Wu, and H. Liu, "An attenuation-partition based iterative phase retrieval algorithm for in-line phase-contrast imaging," Opt. Express **16**, 13330–13341 (2008).
[14]P. Cloetens, R. Mache, M. Schlenker, and S. Lerbs-Mache, "Quantitative phase tomography of Arabidopsis seeds reveals intercellular void network," Proc. Natl. Acad. Sci. **103**, 14626–14630 (2006).
[15]T. Gureyev, D. Paganin, G. Myers, Ya. Nesterets, and S. Wilkins, "Phase-and-amplitude computer tomography," Appl. Phys. Lett. **89**(1–3), 034102 (2006).
[16]X. Wu, H. Liu, and A. Yan, "Phase-contrast x-ray tomography: Contrast mechanism and roles of phase retrieval," Eur. J. Radiol. **68**, S8–S12 (2008).
[17]X. Wu and H. Liu, "Phase-space evolution of x-ray coherence in phase-sensitive imaging," Appl. Opt. **47**, E44–E52 (2008).
[18]A. Yan, X. Wu, and H. Liu, "Performance analysis of the attenuation-partition based iterative phase retrieval algorithm for in-line phase-contrast imaging," Opt. Express **18**, 16074–16089 (2010).
[19]N. A. Dyson, *X-rays in Atomic and Nuclear Physics* (Essex, UK, 1973).
[20]X. Wu, H. Liu, and A. Yan, "X-ray phase-attenuation duality and phase retrieval," Opt. Lett. **30**, 379–381 (2005).
[21]M. Born and E. Wolf, *Principle of Optics*, 6th ed. (Pergamon, Oxford, 1980).
[22]A. Tikhonov and V. Aresenin, *Solution of Ill-posed Problems* (Winston & Sons, Washington, 1977).
[23]B. D. Arhatari, K. Hannah, E. Balaur, and A. G. Peele, "Phase imaging using a polychromatic x-ray laboratory source," Opt. Express **16**, 19950–19956 (2008).
[24]D. Paganin, S. C. Mayo, T. E. Gureyev, P. Miller, and S. W. Wilkins, "Simultaneous phase and amplitude extraction from a single defocused image of a homogeneous object," J. Microscopy **206**, 33–40 (2002).

Nuclear Instruments and Methods in Physics Research B 269 (2011) 1841–1843

Contents lists available at ScienceDirect

Nuclear Instruments and Methods in Physics Research B

journal homepage: www.elsevier.com/locate/nimb

Short Communication

Apparent linear attenuation coefficients in phase contrast X-ray tomography

Aimin Yan, Xizeng Wu *

Department of Radiology, University of Alabama at Birmingham, 619 19th St. South, GSB 301 Birmingham, AL 35249, USA

ARTICLE INFO

Article history:
Received 20 April 2011
Received in revised form 11 May 2011
Available online 20 May 2011

Keywords:
X-ray phase contrast imaging
X-ray tomography

ABSTRACT

In the inline phase contrast X-ray tomography the reconstructed apparent linear attenuation coefficient values may be greatly larger than sample's linear attenuation coefficients or even be negative. In this work we present a general formula to quantitatively relate the apparent linear attenuation coefficient values in cone-beam phase contrast tomography to sample's linear attenuation coefficients and refractive indices. This formula overcomes the gross inaccuracy of the existing formula in the literature in analyzing high-resolution phase contrast tomography, and it will be useful for correctly interpreting and quantifying the apparent linear attenuation coefficients in cone-beam X-ray phase contrast tomography.

For many applications the X-ray attenuation contrast, such as mass–density differences between different material components, is too small to generate enough image contrast with conventional X-ray tomography. Taking advantage of highly sensitive X-ray phase shifts generated from X-ray coherent scattering, phase contrast X-ray tomography finds broad applications in material science and engineering, biomedical imaging and many other scientific fields [1–3]. In phase contrast X-ray tomography one first makes phase contrast angular projections, in which the refraction and diffraction of phase shifted X-rays form the edge-enhancing interference fringes at interfaces of different material components. From these angular projections 3-D tomograms are then reconstructed using the standard tomography reconstruction methods such as the filtered backprojection methods. The reconstructed phase-sensitive tomograms exhibit enhanced interfaces and layers of different materials and tissues [1–3]. However, these tomograms are not the maps of the linear attenuation coefficients (LACs) of the sample, rather they are the maps of the reconstructed apparent LACs, which may present anomalously large or even negative apparent LAC values at interfaces between different materials and tissues. These "artifacts" may cause faulty interpretation of sample structures, and impede even qualitative characterizations for tissues and materials [1,2,4–6]. As a result, for example, the apparent LAC values of small bronchi were found lower than that of air in phase contrast tomography experiments [2]. In order to correctly interpret and quantify the mixed contrast exhibited in phase contrast tomography, it is necessary to find out quantitative relations between the apparent LAC, on the one hand, and the actual LAC and refractive index, on the other. The previous studies found that the apparent LAC $\mu_{\text{apparent}}(\vec{r}_0)$ in X-ray phase contrast tomography is given by [7–9]:

$$\mu_{\text{apparent}}(\vec{r}_0) = \mu(\vec{r}_0) - \frac{R_2}{M}\cdot\left(\frac{\partial^2}{\partial x_1^2}+\frac{\partial^2}{\partial x_2^2}+\frac{\partial^2}{\partial x_3^2}\right)\Delta_{\text{refr}}(\vec{r}_0). \quad (1)$$

In this equation the first additive term $\mu(\vec{r}_0)$denotes the sample's actual LAC value at position $\vec{r}_0$, and the second additive term is proportional to the three-dimensional Laplacian of the sample's refractive index decrement $\Delta_{\text{refr}}(\vec{r}_0)$ [7–9]. In Eq. (1) R_2 denotes the sample-detector distance and M the magnification factor employed in angular projections. In the literature this second term is used to explain the edge enhancement and the anomalous values of large apparent LAC [7–9].

However, in high-resolution phase contrast tomography with micrometer-scale resolutions the applicability of Eq. (1) is called into question. Researchers recently found that Eq. (1) is invalid in some synchrotron radiation microtomography experiments [10]. In fact, in the derivation of Eq. (1) the phase-sensitive projections were modeled based on the so-called Transport of Intensity Equation (TIE) [7–9]. The TIE describes how the phase-shifted X-rays refract and diffract to form interference fringes at boundaries of material components [11,12]. However, we noted that TIE can only describe the moderate-resolution phase-sensitive projections with $\pi\lambda R_2/(4M\sigma^2) << 1$, where σ denotes the finest size resolved. In cases of high-resolution projections with micrometer-scale resolutions, the fine size resolved could be so small such that $\pi\lambda R_2/4M\sigma^2 \sim 1$ or larger, then TIE becomes inapplicable and Eq. (1) cannot quantify the apparent LAC values observed in high-resolution phase contrast tomography.

To overcome the limitations of Eq. (1), we derived a novel and general formula of apparent LAC values in phase contrast X-ray tomography. Instead of using the TIE, in the derivation we employed the general phase-sensitive projection formula that is

* Corresponding author. Tel.: +1 205 975 8135; fax: +1 205 975 4679.
E-mail addresses: ayan@uabmc.edu (A. Yan), xwu@uabmc.edu (X. Wu).

0168-583X/$ - see front matter © 2011 Elsevier B.V. All rights reserved.
doi:10.1016/j.nimb.2011.05.018

applicable for high-resolution projections as well [13–14]. We then applied the standard Feldkamp–Davis–Kresss (FDK) cone-beam reconstruction algorithm to the ray-sums of phase-sensitive angular projections [15]. We found that the apparent LAC value $\mu_{\text{apparent}}(\vec{r}_0)$ is given by

$$\mu_{\text{apparent}}(\vec{r}_0) = \cos\left(\frac{\lambda R_2}{4\pi M}\nabla_{3D}^2\right)\mu(\vec{r}_0) - \frac{4\pi}{\lambda} \times \sin\left(\frac{\lambda R_2}{4\pi M}\nabla_{3D}^2\right)\Delta_{\text{refr}}(\vec{r}_0), \quad (2)$$

where the three-dimensional Laplacian operator $\nabla_{3D}^2 \equiv (\partial^2/\partial x_1^2 + \partial^2/\partial x_2^2 + \partial^2/\partial x_3^2)$. The operators $\sin\left((\lambda R_2/4\pi M)\nabla_{3D}^2\right)$ and $\cos((\lambda R_2/4\pi M)\nabla_{3D}^2)$ in above equation are the pseudo-differential operators. The action of a pseudo-differential operator such as $\sin(c\nabla_{3D}^2)$ on a function $g(\vec{r}_0)$ is defined as $\sin(c\nabla_{3D}^2)g(\vec{r}_0) \equiv \int\int \exp(i2\pi(\vec{r}-\vec{r}_0)\cdot\vec{f})\cdot\sin\left(-4\pi^2 c\vec{f}^2\right)g(\vec{r})d^3\vec{r}d^3\vec{f}$. Note that Eq. (2) is indeed a generalization of Eq. (1). For experiments with moderate-resolutions or short sample-detector distances such that $\pi\lambda R_2/4M\sigma^2 << 1$, we then have $\cos((\lambda R_2/4\pi M)\nabla_{3D}^2) \approx 1$ and $\sin((\lambda R_2/4\pi M)\nabla_{3D}^2) \approx (\lambda R_2/4\pi M)\nabla_{3D}^2$. Thereby the first term on the RHS of Eq. (2) reduces to the actual LAC, the second term to a scaled Laplacian of $\Delta_{\text{refr}}(\vec{r}_o)$ and Eq. (2) recovers Eq. (1), as is expected.

In order to validate Eq. (2), we performed numerical simulations. In the simulations the X-ray source was a point source of 60 keV X-rays. The LACs and refractive indices of the numerical phantom were constructed as the sums of the LACs and refractive indices of six spheres of light elements with different radii and center positions. For each sphere the mass densities were designed to decrease radially and diminish rapidly at the sphere's boundary for generating phase contrast. Specifically we set $\mu(\vec{r}_0) = 0.215\times\sum_{n=1}^{6} f_n(\vec{r}_0)(1/\text{cm})$ and $\Delta_{\text{refr}}(\vec{r}_0) = (7.548\times10^{-8})\times\sum_{n=1}^{6} f_n(\vec{r}_0)$, where $f_n(\vec{r}_0) = \sqrt{R_n^2 - (\vec{r}_0-\vec{r}_n)^2}/4R_n$ if $|(\vec{r}_0-\vec{r}_n)| \leqslant R_n$ and $f_n(\vec{r}_0) = 0$ otherwise. Here $\vec{r}_n$ and R_n ($n = 1, 2, \ldots, 6$) denote the center position and radius of the respective sphere. In this way the LACs and refractive indices change continuously without any steps but vary rapidly at the sphere boundaries. Hence strong phase contrast would manifest around the boundaries of the spheres. The detector has 512×512 pixels with a sampling pitch of 2 μm. In the simulated scan the source traced a circle orbit, and the source and detector rotated together over an angular range of 360° in 0.5° steps. In order to simulate X-ray Fresnel diffractions involved in the angular projections, one needs to compute X-ray attenuation values and phase shifts of the exit rays in each of the projections. In general one needs to use the multislice propagation method to account for X-ray Fresnel diffractions inside the sample [16]. However, the settings described above satisfy the so-called thin object condition $T < p^2/2\lambda_0$, where T denotes the sample's thickness, p is the resolution and λ_0 the wavelength of 60 keV X-ray [16]. This

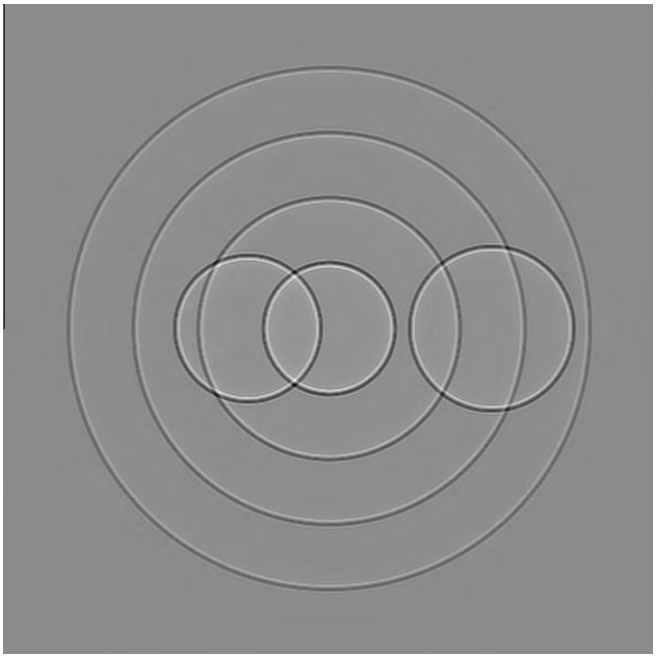

Fig. 1. Reconstructed apparent LAC map of a phantom slice from the phase-sensitive cone-beam tomography with mixed contrast.

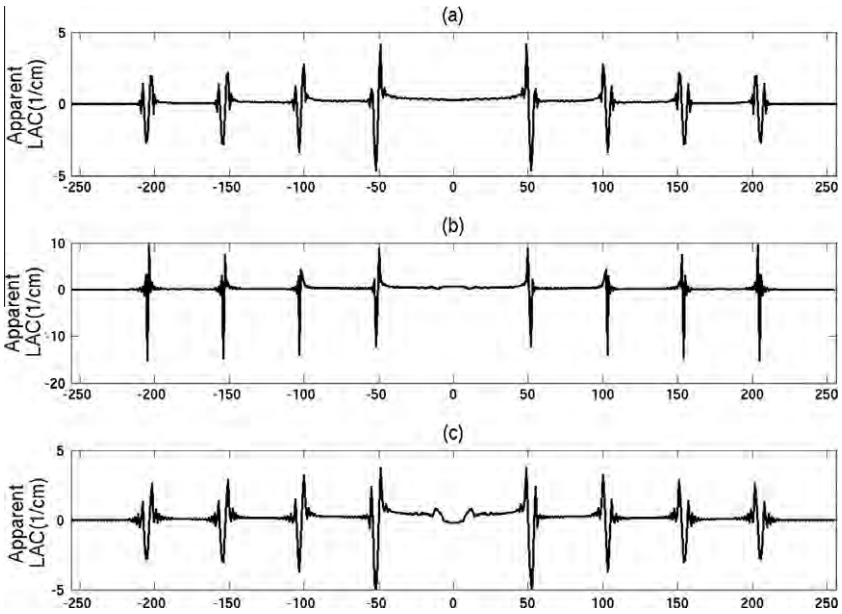

Fig. 2. Profiles of the apparent LACs along the vertical line passing the center of the central sphere. (a) Profile measured from Fig. 1. (b) Profile calculated based on Eq. (1). (c) Profile calculated based on the general formula Eq. (2).

Table 1
A comparison of the fringe peak–peak differences in Fig. 2(a)–(c).

	Fringe set 1	Fringe set 2	Fringe set 3	Fringe set 4	Fringe set 5	Fringe set 6	Fringe set 7	Fringe set 8
Peak–peak difference of apparent LACs in Fig. 2(a) (1/cm)	4.648	4.979	6.098	8.860	8.860	6.098	4.979	4.648
Error of calculated peak–peak difference based on Eq. (1) (Fig. 2(b)) (%)	429	346	199	136	136	199	346	429
Error of calculated peak–peak difference based on Eq. (2) (Fig. 2(c)) (%)	15.0	17.5	13.0	6.9	6.9	13.0	17.5	15.0

condition allows us to compute the X-ray attenuation values and phase shifts of the exit X-rays as the ray integrals of the sample's LACs and refractive index decrements. In this simulation a ray-tracing algorithm was used to compute the ray integrals such as $\int \mu dl$ and $\int \Delta_{refr} dl$ in each of the angular projections. The exit X-ray attenuation and phase shift were determined as $A^2 = \exp\left(-\int \mu dl\right)$ and $\varphi = -(2\pi/\lambda)\int \Delta_{refr} dl$, respectively [11–14]. Using the exit X-ray attenuation and phase shift from a given projection, we then simulated the free-space Fresnel diffractions of the exit X-rays propagating from the sample to the detector with a setting of R_2 = 1 m and M = 2 [16]. The Fresnel diffraction intensities in all the angular projections were log-transformed to calculate the ray-sums needed for tomographic image reconstruction. We applied the standard FDK algorithm for image reconstruction [15]. Fig. 1 shows a reconstructed slice of apparent LAC values in gray scale. This slice shows the edge-enhancing dark–bright fringes caused by phase contrast at the interfaces between the spheres. Fig. 2(a) shows the profile of the apparent LAC values along the vertical central line of Fig. 1. The ordinate denotes apparent LAC value in (1/cm) along the vertical line, while the abscissa denotes pixel location along the line. For the sake of comparison Fig. 2(b) and Fig. 2(c) show the profiles of the apparent LAC values along the vertical line, which were computed by using Eq. (1) and Eq. (2) respectively. Note that the ordinate scale in Fig. 2(b) is three times larger than that of Fig. 2(a) and (c). To facilitate the comparisons of the three profiles, we measured the fringe's peak-to-peak differences (the changes between peak and trough) at eight fringe sets for each of the three profiles shown in Fig. 2(a)–(c). Table 1 lists the measured fringe peak-to-peak differences of apparent LACs in Fig. 2(a), which is obtained from Fig. 1, the phantom's phase contrast tomogram simulated by using the Fresnel diffraction and FDK-reconstruction. Compared to these eight peak-to-peak differences in Fig. 2(a), the table lists as well the errors of the calculated peak–peak differences based on Eq. (1) (Fig. 2(b)) and Eq. (2) (Fig. 2(c)) respectively. From these comparisons, it is clear that the apparent LAC values calculated from Eq. (1) are grossly inaccurate with the errors amounting to several hundred percent, while the apparent LAC values calculated by means of Eq. (2) achieve reasonable quantitative accuracies as is shown in Table 1. In addition, the profile Fig. 2(c) shows two small bumps at the center of the profile. We found that these variations of apparent LACs are artifacts caused by omitting the small nonlinear terms in phase shifts in the derivation of Eq. (2). The omission of these nonlinear terms mainly affects the accuracies in computing the side-lobes of phase contrast fringes, thereby causes these two small bumps, which are associated with the distorted fringe side-lobes near the right boundary of the left off-center sphere in the phantom (Fig. 1).

In summary, we present a general formula (Eq. (2)) to quantitatively relate the apparent LAC values in cone-beam phase contrast tomography to sample's LAC and refractive index values. This formula overcomes the gross inaccuracy of the existing formula in the literature in analyzing high-resolution phase contrast tomography. We believe that this general formula will be useful for designing phase contrast tomography experiments, and for correctly interpreting and quantifying the apparent LAC values in cone-beam X-ray phase contrast tomography. For example, Eq. (2) can be used for computing the edge-enhancement profiles for analyzing presampling modulation transfer functions in synchrotron radiation microtomography [10].

Acknowledgment

This research was supported in part by the NIH Grant R01CA142587 and the DoD Breast Cancer Research Program award W81XWH-08-1-0613.

References

[1] S.R. Stock, Recent advances in X-ray microtomography applied to materials, Int. Mater. Rev. 53 (2008) 129–181.
[2] T. Sera, K. Uesugi, N. Yagi, Refraction-enhanced tomography of mouse and rabbit lungs, Med. Phys. 32 (2005) 2787–2792.
[3] W. Zhu, G. Gaetani, F. Fusseis, L. Montési, F. De Carlo, Microtomography of partially molten rocks: three-dimensional melt distribution in mantle peridotite, Science 332 (2011) 88–91.
[4] S. Mayo, T. Davis, T. Gureyev, P. Miller, D. Paganin, A. Pogany, A. Stevenson, S. Wilkins, X-ray phase-contrast microscopy and microtomography, Opt. Express 11 (2003) 2289–2302.
[5] E. Donnelly, R. Price, K. Lewis, D. Pickens, Polychromatic phase-contrast computed tomography, Med. Phys. 34 (2007) 3165–3168.
[6] Y. De Witte, M. Boone, J. Vlassenbroeck, M. Dierick, L. Van Hoorebeke, Bronnikov-aided correction for X-ray computed tomography, J. Opt. Soc. Am. A26 (2009) 890–894.
[7] P. Cloetens, M. Pateyron-Salome, J. Buffiere, G. Peix, J. Baruchel, F. Peyrin, M. Schlenker, Observation of microstructure and damage in materials by phase sensitive radiography and tomography, J. Appl. Phys. 81 (1997) 5878–5886.
[8] X. Wu, H. Liu, A. Yan, Phase-contrast X-ray tomography: contrast mechanism and roles of phase retrieval, Eur. J. Radiol. 68 (2008) S8–S12.
[9] W. Cai, R. Ning, Preliminary study of a phase-contrast cone-beam computed tomography system: the edge-enhancement effect in the tomographic reconstruction of in-line holographic images, Opt. Eng. 47 (2008) 1–12. 037004.
[10] R. Mizutani, K. Taguchi, A. Takeuchi, K. Uesugi, Y. Suzuki, Estimation of presampling modulation transfer function in synchrotron radiation microtomography, Nucl. Instrum. Meth. A 621 (2010) 615–619.
[11] M. Teague, Deterministic phase retrieval: a Green's function solution, J. Opt. Soc. Am. 73 (1983) 1434–1441.
[12] K. Nugent, T. Gureyev, D. Cookson, D. Paganin, Z. Barnea, Quantitative phase imaging using hard X-rays, Phys. Rev. Lett. 77 (1996) 2961–2965.
[13] X. Wu, H. Liu, A general theoretical formalism for X-ray phase contrast imaging, J. X-Ray Sci. Technol. 11 (2003) 33–42.
[14] J. Guigay, M. Langer, R. Boistel, P. Cloetens, Mixed transfer function and transport of intensity approach for phase retrieval in the Fresnel region, Opt. Lett. 32 (2007) 1617–1619.
[15] L. Feldkamp, C. Davis, J. Kress, Practical cone-beam algorithm, J. Opt. Soc. Am. A1 (1984) 612–619.
[16] J. Cowley, Diffraction Physics, 3rd ed., North-Holland, Amsterdam, 1995.